Four-body extension of the continuum-discretized coupled-channels method

P. Descouvemont*

Physique Nucléaire Théorique et Physique Mathématique, C.P. 229, Université Libre de Bruxelles (ULB), B-1050 Brussels, Belgium

(Received 11 March 2018; published 11 June 2018)

I develop an extension of the continuum-discretized coupled-channels (CDCC) method to reactions where both nuclei present a low breakup threshold. This leads to a four-body model, where the only inputs are the interactions describing the colliding nuclei, and the four optical potentials between the fragments. Once these potentials are chosen, the model does not contain any additional parameter. First I briefly discuss the general formalism, and emphasize the need for dealing with large coupled-channel systems. The method is tested with existing benchmarks on 4α bound states with the Ali-Bodmer potential. Then I apply the four-body CDCC to the $^{11}\mathrm{Be}+d$ system, where I consider the $^{10}\mathrm{Be}(0^+,2^+)+n$ configuration for ^{11}Be. I show that breakup channels are crucial to reproduce the elastic cross section, but that core excitation plays a weak role. The $^{7}\mathrm{Li}+d$ system is investigated with an $\alpha+t$ cluster model for ^{7}Li. I show that breakup channels significantly improve the agreement with the experimental cross section, but an additional imaginary term, simulating missing transfer channels, is necessary. The full CDCC results can be interpreted by equivalent potentials. For both systems, the real part is weakly affected by breakup channels, but the imaginary part is strongly modified. I suggest that the present wave functions could be used in future DWBA calculations.

DOI: 10.1103/PhysRevC.97.064607

I. INTRODUCTION

The continuum-discretized coupled-channels (CDCC) method was first developed in the 1970s [1]. It was realized that elastic cross sections for deuteron-induced reactions could not be described by standard optical potentials. A significant progress was made possible by introducing breakup states of the deuteron. This lead to the idea of a discretized continuum which was subsequently used by many authors (see, for example, Refs. [2–4] for reviews).

For many years, CDCC calculations involved three-body systems. Typical examples are deuteron + nucleus reactions, where the deuteron is described by a $p+n$ structure. For more than 20 years, the three-body CDCC method was successfully applied to reactions involving weakly bound nuclei, such as ^{11}Be, which can be seen as a $^{10}\mathrm{Be}+n$ system. The CDCC theory represents a natural framework for reactions involving exotic nuclei. The main property of exotic nuclei is their low breakup threshold, and couplings to the continuum are quite important. More recently, the CDCC method was extended to reactions involving three-body projectiles, such as ^{6}He [5], ^{9}Be [6], or ^{11}Li [7]. Going from two-body to three-body projectiles represents a strong increase in the complexity of numerical calculations: The three-body continuum involves larger level densities, and the calculation of the coupling potentials is more time consuming.

Until now, most scattering calculations use the assumptions that the target remains in its ground state. This is certainly a fair approximation for heavy targets, but is more questionable for light targets. A typical example is the deuteron, which is used as a target for the investigation of exotic nuclei by stripping reactions (see, for example, Ref. [8]). If the projectile also presents a two-body structure, current versions of the CDCC method are no longer sufficient. In this work, I present a new extension of CDCC, where the breakup of both colliding nuclei is included. I assume a two-body structure for the projectile and for the target, which leads to a four-body model.

The aim of the CDCC method is essentially to investigate reactions. However, this framework is also able to describe bound states. I use this property to test the model with the 4α system, which was studied in the literature [9,10] by more specific few-body methods. This application not only provides a numerical test of the model, but also allows one to analyze the convergence of 4α bound-state energies.

A typical application of the four-body model is the $^{11}\mathrm{Be}+d$ reaction, which was experimentally studied recently [11]. In this reaction, ^{11}Be and the deuteron present a low breakup threshold, and four-body breakup effects are expected to be important. First results were presented in Ref. [12], and are extended here by including core excitation of ^{10}Be. Another natural application of a four-body model is the $^{7}\mathrm{Li}+d$ reaction, because ^{7}Li is known to have an $\alpha+t$ cluster structure.

The paper is organized as follows. In Sec. II, I briefly present the model, by emphasizing specific aspects of the four-body calculations. Section III is devoted to the 4α system, where bound states are computed. In Secs. IV and V, I present the $^{11}\mathrm{Be}+d$ and $^{7}\mathrm{Li}+d$ cross sections, respectively. As CDCC calculations involve many channels, it is useful to have equivalent, single-channel potentials. Such potentials can be derived approximately, and give a more intuitive interpretation of the full calculations; they are presented in Sec. VI. Conclusions and outlook are given in Sec. VII.

*pdesc@ulb.ac.be

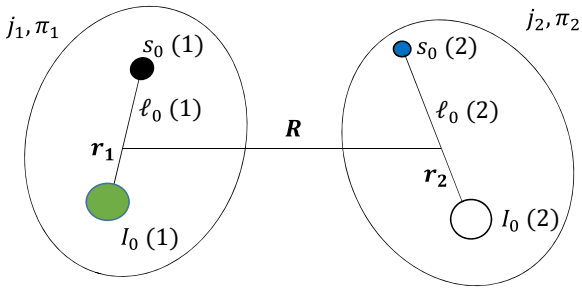

FIG. 1. Cluster configuration and coordinates used in the four-body model.

II. THE CDCC FOUR-BODY MODEL

A. General presentation

The goal of the present work is to extend the CDCC formalism to systems involving two nuclei with a low breakup threshold. This situation is typical of deuteron-induced reactions on exotic nuclei. As the deuteron cannot be considered as an inert system, a four-body model is necessary if the exotic nucleus (such as ^{11}Be, ^{8}B, or ^{19}C) also presents a low separation energy. Further extensions to three-body projectiles have been considered [5–7], but with structureless targets.

Let me consider the four-body system of Fig. 1. The coordinates $\boldsymbol{r}_1$ and $\boldsymbol{r}_2$ describe the internal motion of the colliding nuclei, whereas $\boldsymbol{R}$ is associated with the relative motion. Although other coordinate choices are possible for four-body systems [13], those adopted here are well suited to scattering problems. The total Hamiltonian is given by

$$H = T_R + H_1(\boldsymbol{r}_1) + H_2(\boldsymbol{r}_2) + V(\boldsymbol{R},\boldsymbol{r}_1,\boldsymbol{r}_2), \tag{1}$$

where T_R is the relative kinetic energy and potential V is defined from four optical potentials as

$$V(\boldsymbol{R},\boldsymbol{r}_1,\boldsymbol{r}_2) = \sum_{i=1}^{2}\sum_{j=1}^{2} V_{ij}^0(\boldsymbol{R},\boldsymbol{r}_1,\boldsymbol{r}_2). \tag{2}$$

As usual in CDCC calculations, interaction V_{ij}^0 is chosen to optimize the scattering properties of the $i+j$ subsystem. For nucleon + target systems, several compilations are available in the literature [14,15]. Nucleus-nucleus potentials are sometimes known from experiment (such as ^{10}Be + ^{64}Zn [16], for example), or are estimated from folding procedures (such as d + ^{10}Be [11], for example).

In Eq. (1), H_1 and H_2 represent the internal Hamiltonian of the colliding nuclei, and are given by

$$H_i(\boldsymbol{r}_i) = t_i + v_i(\boldsymbol{r}_i), \tag{3}$$

where t_i is the two-body kinetic energy, and $v_i(\boldsymbol{r}_i)$ a two-body (real) potential chosen to reproduce important properties (energies, radii, etc.) of the nucleus. Neglecting the tensor force, potential $v_i(\boldsymbol{r}_i)$ is defined as

$$v_i(\boldsymbol{r}_i) = V_N(r_i) + V_C(r_i) + \boldsymbol{\ell}\cdot\boldsymbol{s}\, V_{\ell s}(r_i), \tag{4}$$

where V_N, V_C, and $V_{\ell s}$ are nuclear, Coulomb and spin-orbit terms, respectively. In many CDCC calculations, core excitations are neglected, and the form factors are radial (typical forms are Gaussian or Woods-Saxon potentials). It was shown, however, that core excitation may be important in nuclei such as ^{11}Be [17] or ^{19}C [18]. This extension of CDCC is known as the XCDCC method [19]. Owing to the deformation, the radius where the potential is evaluated is modified by a shift [20] as

$$V(r) \to V(r - \delta(\theta)), \tag{5}$$

with the multipole expansion,

$$\delta(\theta) = \sum_{\lambda>0} \delta_\lambda Y_\lambda^0(\theta,0). \tag{6}$$

In general this expansion is limited to $\lambda = 2$, i.e., to quadrupole deformations.

In the presence of deformation, the two-body potentials are expanded in multipoles as

$$V(\boldsymbol{r}) = \sum_\lambda (2\lambda+1) v_\lambda(r) P_\lambda(\cos\theta), \tag{7}$$

where the radial components,

$$v_\lambda(r) = \frac{1}{2}\int_0^\pi V(\boldsymbol{r}) P_\lambda(\cos\theta) d(\cos\theta), \tag{8}$$

are evaluated numerically. These definitions are valid for the nuclear as well as for the Coulomb terms.

B. Two-body wave functions

The first step in all CDCC calculations is to solve the Schrödinger equation (3) associated with the colliding nuclei,

$$H_i\, \Phi_{i,k}^{j\pi} = E_{i,k}^{j\pi}\, \Phi_{i,k}^{j\pi}, \tag{9}$$

where $(j\pi)$ are the spin and parity, and k is the excitation level in nucleus i. The two-body wave function of nucleus i is then factorized as

$$\Phi_k^{j\pi}(\boldsymbol{r}) = \sum_{I_0\ell_0 j_0} u_{k,I_0\ell_0 j_0}^{j\pi}(r)\varphi_{k,I_0\ell_0 j_0}^{j\pi}(\Omega_r). \tag{10}$$

This summation involves the spin of the core I_0, the relative angular momentum ℓ_0, and its coupling to the spin s_0 of the second fragment (see Fig. 1). For the sake of clarity, I drop index i and use labels $c = (j,\pi,k)$ and $\gamma = (I_0,\ell_0,j_0)$. The angular function φ_γ^c is given by

$$\varphi_\gamma^c(\Omega_r) = [\Phi_{I_0} \otimes [Y_{\ell_0}(\Omega_r) \otimes \Phi_{s_0}]^{j_0}]^j, \tag{11}$$

where Φ_{I_0} and Φ_{s_0} are spinors associated with the two fragments. Two options are possible for the radial functions $u_\gamma^c(r)$: Either they are obtained from a diagonalization of Hamiltonian (3), or they are defined from "bins." Both techniques are known to provide equivalent results for the scattering process [21].

In the first alternative the radial functions are expanded over a set of N basis functions $f_n(r)$ as

$$u_\gamma^c(r) = \sum_{n=1}^{N} d_{\gamma n}^c f_n(r), \tag{12}$$

where coefficients $d^c_{\gamma n}$ are obtained from the eigenvalue problem,

$$\sum_{\gamma' n'} \langle f_n \varphi^c_\gamma | H_i - E^c | f_{n'} \varphi^c_{\gamma'} \rangle d^c_{\gamma' n'} = 0. \quad (13)$$

This system must be solved for each $j\pi$ considered in the nucleus. Energies E^c (defined from the breakup threshold) represent physical states ($E^c < 0$), or approximations of continuum states ($E^c > 0$), also referred to as pseudostates. A brief discussion of the resolution of (13) with Lagrange functions [22] is presented in Appendix A.

C. Nucleus-nucleus scattering

The next step in the CDCC formalism is to solve the four-body Schrödinger equation at the scattering energy E,

$$H \Psi^{JM\pi}_\omega = E \Psi^{JM\pi}_\omega, \quad (14)$$

where the Hamiltonian H is given by Eq. (1), and where ω is the entrance channel. The wave function is expanded as

$$\Psi^{JM\pi}_\omega = \sum_{c_1 c_2 L I} \varphi^{JM\pi}_{c_1 c_2 L I}(\Omega_R, \boldsymbol{r}_1, \boldsymbol{r}_2)\, g^{J\pi}_{c_1 c_2 L I(\omega)}(R), \quad (15)$$

where the channel function is defined by

$$\varphi^{JM\pi}_\alpha = \left[\left[\Phi^{c_1}_1(\boldsymbol{r}_1) \otimes \Phi^{c_2}_2(\boldsymbol{r}_2) \right]^I \otimes Y_L(\Omega_R) \right]^{JM}. \quad (16)$$

In this definition, I is the channel spin, L is the relative angular moment, and I use $\alpha = (c_1 c_2 L I)$. The L values are limited by angular momentum couplings, and by the condition on the parity $\pi = \pi_1 \pi_2 (-1)^L$. The summation over c_1 and c_2 is limited by a truncation energy $E_{\max}$ and by a truncation angular momentum $J_{\max}$ (these limits may be different for both nuclei). As usual in CDCC calculations, numerical tests must be performed to ensure the convergence of the cross sections.

In Eq. (15) the long-range behavior of the radial functions is given by

$$g^{J\pi}_{\alpha(\omega)} \longrightarrow \frac{1}{\sqrt{v_\alpha}} \left(\delta_{\alpha\omega} I_\alpha(k_\alpha R) - U^{J\pi}_{\alpha\omega} O_\alpha(k_\alpha R) \right), \quad (17)$$

where $I_\alpha(x)$ and $O_\alpha(x)$ are the incoming and outgoing Coulomb functions, v_α is the relative velocity, and $\boldsymbol{U}^{J\pi}$ is the scattering matrix. I assume here that all channels are open; a generalization to closed channels can be found in Refs. [23,24]. Functions $g^{J\pi}$ are obtained from the standard coupled-channel system,

$$\left[-\frac{\hbar^2}{2\mu} \left(\frac{d^2}{dR^2} - \frac{L(L+1)}{R^2} \right) + E^{c_1}_1 + E^{c_2}_2 - E \right] g^{J\pi}_{\alpha(\omega)} + \sum_{\alpha'} V^{J\pi}_{\alpha\alpha'} g^{J\pi}_{\alpha'(\omega)} = 0, \quad (18)$$

where μ is the reduced mass, and where the coupling potentials are defined from matrix elements of potential (2) as

$$V^{J\pi}_{\alpha\alpha'}(R) = \langle \varphi^{JM\pi}_\alpha | \sum_{ij} V^0_{ij} | \varphi^{JM\pi}_{\alpha'} \rangle. \quad (19)$$

These matrix elements involve integrals over $\boldsymbol{r}_1$,$\boldsymbol{r}_2$, and Ω_R, which means eight-dimensional integrals. The integrals over Ω_R are performed analytically. For the integration over $\boldsymbol{r}_1$ and $\boldsymbol{r}_2$, the angular parts are obtained from numerical quadratures, and the radial parts are greatly simplified by the use of Lagrange functions. Details on the calculations of the coupling potentials are given in Appendix B.

The main issue in the present four-body model is not the calculation of the coupling potentials (19). Although this can be time-consuming, the main challenge of the model is to solve the coupled-channel system (18) with a large number of channels. In standard CDCC calculations, only one of the colliding nuclei may be broken up. Although the number of pseudostates or bins can be quite large, the other colliding nucleus remains in its ground state. The present model goes beyond this limitation, as both nuclei may break up. In practice, this means that the number of channels is the product of the numbers of pseudostates in both nuclei. This extension is necessary in some conditions, such as in reactions involving a deuteron and an exotic nucleus, but it raises the problem of an extremely large number of channels (typically up ∼2000).

I use the R-matrix theory to solve system (18) and to determine the scattering matrix (17). Associated with Lagrange basis functions, the R-matrix model is an efficient tool for scattering problems. The radial wave functions are expanded as

$$g^{J\pi}_{\alpha(\omega)} = \sum_{m=1}^{N_f} D^{J\pi}_{\alpha(\omega),m} F_m(R), \quad (20)$$

where $F_m(R)$ are N_f Lagrange functions associated with Legendre polynomials. General references can be found in Refs. [25,26], and more specific applications in nuclear physics can be found in Refs. [23,24].

III. TEST WITH THE 4α SYSTEM

The present model essentially aims at investigating nucleus-nucleus scattering, with both nuclei presenting a cluster structure. However, basis functions (15) can also be used to study bound states of a four-body system. Although the model is not optimized for this application, bound-state calculations can be compared with existing benchmarks in the literature.

As an application to bound-state calculations, I consider the 4α system, which was investigated in different methods [9,10]. The comparison therefore provides a strong test of the present coupling potentials (19). The $\alpha + \alpha$ potential is the ℓ-independent Ali-Bodmer potential [27], defined as

$$V^N_{\alpha+\alpha}(r) = v_1 \exp(-(r/r_1)^2) + v_2 \exp(-(r/r_2)^2), \quad (21)$$

with $v_1 = 500$ MeV, $r_1 = 0.7$ fm, $v_2 = -130$ MeV, and $r_2 = 2.105$ fm. According to Refs. [9,10], I use $\hbar^2/m_\alpha = 10.4465$ MeV fm^2. In a first step, the Coulomb interaction is neglected.

The energy of the 4α system is shown in Fig. 2 as a function of the truncation energy in ^{8}Be, $E_{\max}$, and of the truncation angular momentum $\ell_{\max}$. With this potential, the 2α and 3α binding energies are −1.37 and −5.12 MeV, respectively [28]. For $J = 0^+$, the calculation predicts two bound states. In each case, the convergence with $\ell_{\max}$ is slow. Using only $\ell_{\max} = 0$ provides a poor approximation. At least $\ell_{\max} = 4$ is necessary. Also, pseudostates up to $E_{\max} \approx 30$ MeV need to be

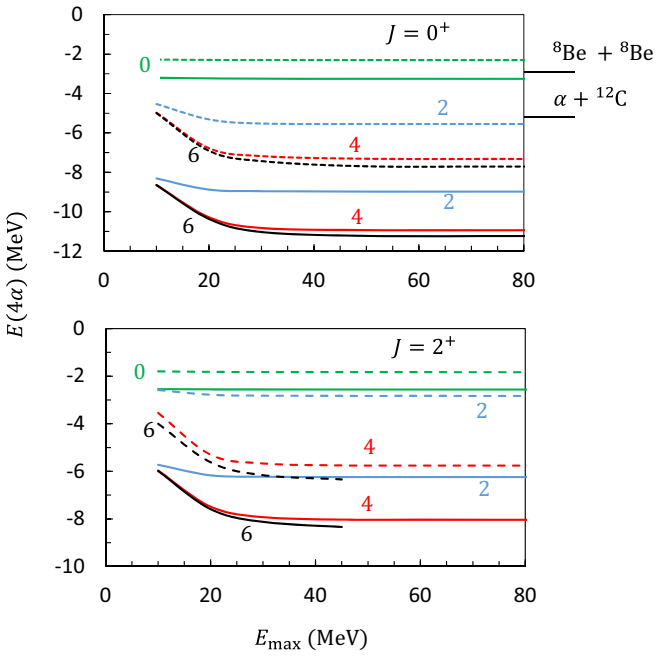

FIG. 2. Energy of the 4α system with the Ali-Bodmer potential [27] for $J = 0^+$ (upper panel) and $J = 2^+$ (lower panel), by neglecting the Coulomb potential. The labels indicate $\ell_{\max}$, the maximum angular momentum in the $\alpha + \alpha$ system. The ^{8}Be + ^{8}Be and $\alpha + {}^{12}$C thresholds are shown on the right of the figure.

included to be close to the exact energy. At convergence, I find $E^{0^+} = -11.23$ MeV. This value is an excellent agreement with the result of Timofeyuk [10] who uses hyperspherical coordinates. Suzuki and Takahashi [9] use the Stochastic Variational Method with Jacobi coordinates and find $E^{0^+} = -11.17$ MeV. This value, however, was recently revised to -11.23 [29]. I find a second eigenvalue at $E^{0^+} = -7.71$ MeV. The convergence for $J = 2^+$ is quite similar to the behavior of $J = 0^+$. I could not reach the same precision because of computer memory limitations. The eigenvalue is $E^{2^+} \approx -8.3$ MeV

In a second step, I include the Coulomb $\alpha - \alpha$ potential,

$$V^C_{\alpha+\alpha}(r) = \frac{4e^2}{r}\mathrm{erf}\left(\frac{r}{r_C}\right), \tag{22}$$

with $r_C = 1.663$ fm. The results are presented in Fig. 3. As it is well known for ^{12}C [28], the Ali-Bodmer potential does not provide a realistic description of the 3α and 4α systems. The experimental ground-state energy of ^{16}O is -14.44 MeV. As for ^{12}C, the potential strongly underestimates the binding energy. However, its simplicity offers an excellent benchmark for four-body calculations.

IV. APPLICATION TO ^{11}Be + d SCATTERING

A. Conditions of the calculations

Data on ^{11}Be + d elastic scattering and breakup have been available recently at a ^{11}Be beam energy $E/A = 26.9$ MeV [11], and first CDCC results were presented in Ref. [12].

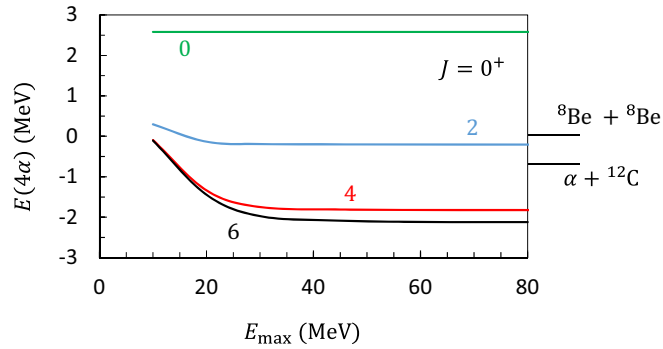

FIG. 3. See caption of Fig. 2 for $J = 0^+$ and by including the Coulomb $\alpha + \alpha$ potential (22).

The ^{11}Be + d system is an ideal candidate for the four-body CDCC method. Both colliding nuclei present a low separation energy (0.50 and 2.22 MeV, respectively). In d+nucleus and ^{11}Be+nucleus scattering, breakup effects of the deuteron and of ^{11}Be are known to be important.

In the present work, I complement the results of Ref. [12] by including ^{10}Be core excitation. For the ^{10}Be + n system, I use two different potentials: (i) as in Ref. [12] the potential of Ref. [30] which neglects ^{10}Be excitation; (ii) the set-I potential of Ref. [31] which includes the ^{10}Be$(2^+) + n$ channel. The latter potential is characterized by a deformation length $\delta_2 = 1.66$ fm, and involves the 2^+ first excited state at $E_x = 3.37$ MeV. In these conditions, the ^{10}Be$(2^+) + n$ component is 15% in the ground state, and 22% in the first excited state. Both potentials reproduce the experimental energies of the $1/2^+$ ground state and of the $1/2^-$ excited state. Potential (1) overestimates the $B(E1, 1/2^- \to 1/2^+)$ value (0.23 e^2.fm^2), whereas potential (2) provides 0.14 e^2 fm^2, in better agreement with experiment (0.102(2) and 0.098(4) e^2 fm^2; see Ref. [32]). For the average distance between ^{10}Be and the neutron, they provide $\sqrt{\langle r^2\rangle} = 6.70$ fm and 6.19 fm, respectively. These values are similar, and close to the experimental value deduced by laser spectroscopy ($\sqrt{\langle r^2\rangle} = 7$ fm [33]). For the $p + n$ system, I use the Minnesota interaction [34], which reproduces the deuteron binding energy, and low-energy scattering properties.

For the ^{10}Be + n and $p + n$ bases, I use Gauss-Laguerre functions with a typical scale factor $h = 0.4$ fm. The number N of basis functions is typically $N = 20$. For ^{10}Be + n, I include angular momenta $j = 1/2^{\pm}, 3/2^{\pm}, 5/2^+$ and $j = 0^+, 2^+$ are considered for $p + n$. Pseudostates up to 20 MeV are included. To compute the cross sections, I use a maximum angular momentum $J_{\max} = 71/2$ which was adopted in Ref. [12]. For the R-matrix conditions, I use a channel radius $a = 25$ fm with $N_f = 50$ Lagrange functions. Various tests have been performed to check the stability of the results against these different parameters.

The model is complemented by four optical potentials between the fragments. For ^{10}Be+nucleon, I use the Koning-Delaroche parametrization [15], and the $n + n$ and $n + p$ potentials are taken as the Minnesota interaction. It was shown in Ref. [12] that the choice of the ^{10}Be+nucleon optical potential has a weak influence on the ^{11}Be + d cross sections

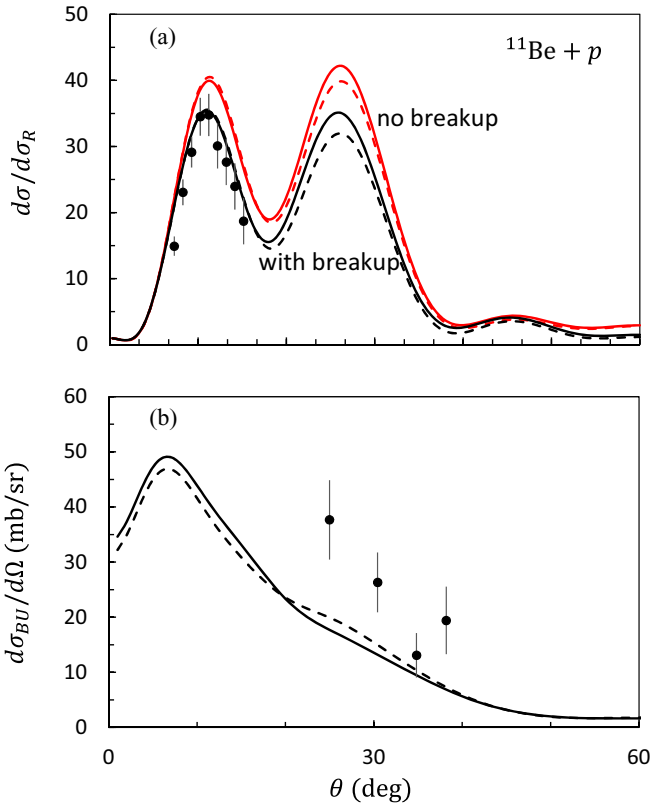

FIG. 4. ^{11}Be + p elastic scattering (a) and breakup (b) cross sections at a ^{11}Be energy $E = 26.9A$ MeV (the elastic cross section is divided by the Rutherford cross section). The solid and dashed lines are obtained with and without core excitation, respectively. The experimental data are taken from Ref. [35].

(less than 5% in the considered angular range, which is much smaller than breakup effects).

B. ^{11}Be + p elastic scattering and breakup

The consistency of the four-body model can be assessed with the ^{11}Be + p subsystem. Data and a CDCC analysis are given in Ref. [35] at the same incident energy $E = 26.9A$ MeV, which corresponds to $E_{\rm c.m.} = 24.7$ MeV.

The elastic cross section is presented in Fig. 4, with the data of Ref. [35]. I use a truncation energy $E_{\rm max} = 10$ MeV; using higher values has a weak effect on the cross section. Figure 4(a) illustrates two effects: the role of the ^{11}Be breakup, and the role of core excitation. As pointed out in Ref. [35], calculations with or without core excitation are fairly similar. The role of ^{11}Be breakup, although weak, is more important. An excellent agreement with the data can be obtained when the ^{11}Be breakup is taken into account. Data at larger angles would be welcome to further test the quality of the model.

In Fig. 4(b), I present the breakup cross section. According to Ref. [35] which detects events from 0.5 to 3 MeV energy between ^{10}Be and n, pseudostates in this energy window are used to determine the CDCC breakup cross section. As for elastic scattering, the role of core excitation is weak,

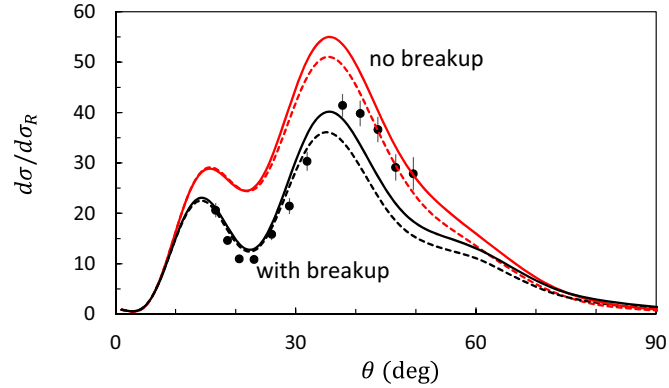

FIG. 5. ^{11}Be + d elastic cross section (divided by the Rutherford cross section) at $E(^{11}\text{Be}) = 26.9A$ MeV, with the single-channel approximation, and with all breakup channels. The solid lines are obtained with core excitation, and the dashed line with the ^{10}Be(0^+) + n configuration only. Tha data are taken from Ref. [11].

and calculations with both potentials underestimate the data. Similar results were obtained in Ref. [35].

C. ^{11}Be + d elastic scattering and breakup

The recent data of Chen *et al.* [11] at a ^{11}Be laboratory energy of $E_{\rm lab} = 26.9A$ MeV correspond to $E_{\rm c.m.} = 45.5$ MeV. The four-body CDCC elastic cross section is presented in Fig. 5. As already mentioned in Ref. [12], the breakup component of the wave function is crucial to reproduce the amplitude of the cross section. With the full CDCC calculation, the minimum near $\theta \approx 20^\circ$ is well reproduced. The single-channel calculation, involving only the ground states of ^{11}Be and of the deuteron, overestimates the data by a factor two at the minimum. Including core excitation of ^{10}Be slightly enhances the cross section for $\theta > 30^\circ$. This goes in the right direction but the calculation is still 10%–20% lower than experiment.

The convergence with respect to the CDCC truncation limits was partly discussed in Ref. [12]. In Fig. 6, I present a more detailed analysis, with the influence of $\ell_{\rm max}$ and of $E_{\rm max}$. For deuteron breakup [Figs. 6(a) and 6(b)], $\ell_{\rm max} = 2$ provides an excellent convergence, as well as $E_{\rm max} = 20$ MeV. In ^{11}Be [Figs. 6(c) and 6(d)], the difference between $\ell_{\rm max} = 2$ and $\ell_{\rm max} = 3$ is negligible and convergence is reached for $E_{\rm max} = 20$ MeV.

Notice that the full calculation involves a very large channel number. With the present numerical conditions, the number of deuteron states is 15, and for ^{11}Be, I have 20 and 38 states for the ^{10}Be(0^+) + n and ^{10}Be(0^+,2^+) + n configurations, respectively. This means that the number of channels reaches values around 600. The size of the coupled-channel system (18) is still larger because I have several channel spins I and several angular momenta L for a given physical channel. The dimension of system (18) is therefore of the order of ∼3000. Such large systems can be solved by the R-matrix method, but they are extremely demanding in terms of computer time and memory. Iterative methods such as those presented in Ref. [36] would allow one to speed up the calculation, but are not applicable here because they assume small channel

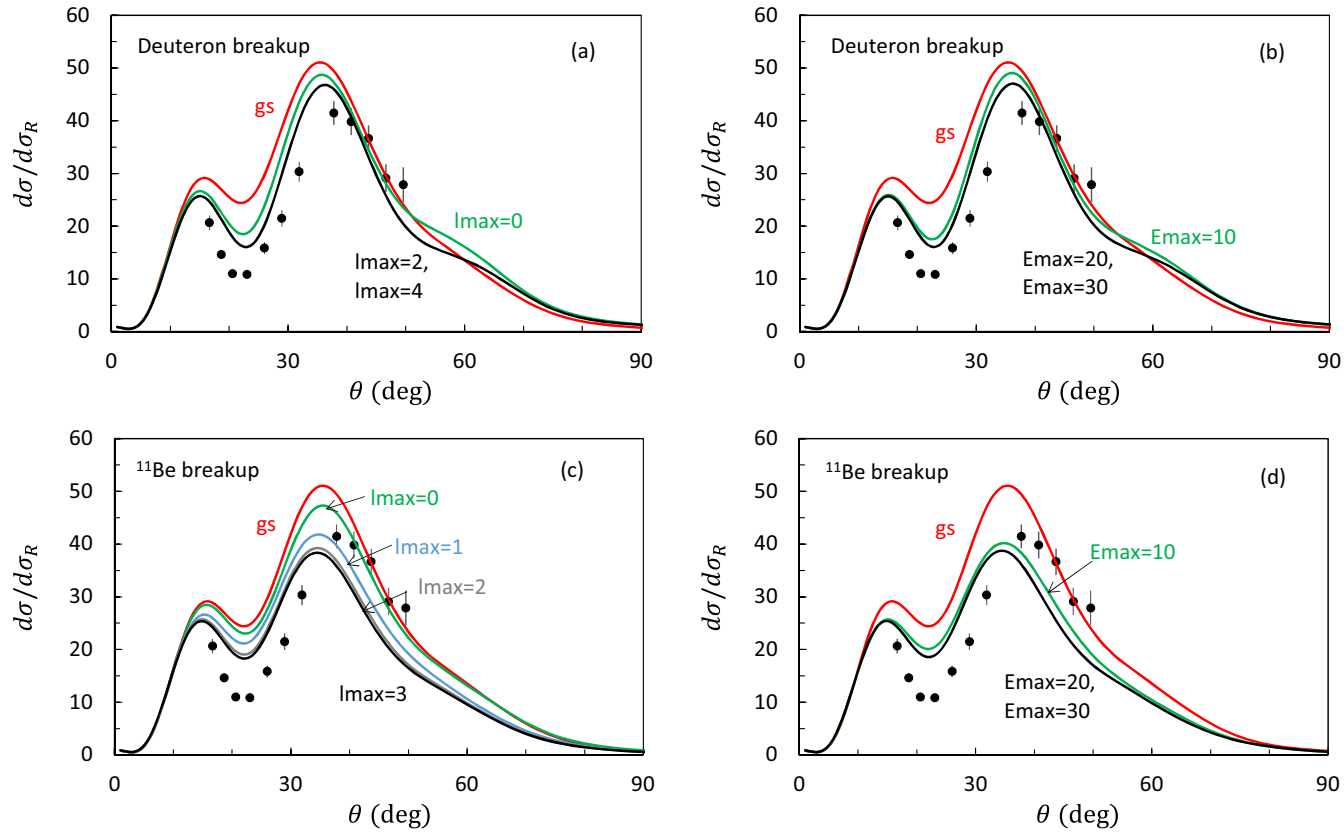

FIG. 6. Convergence of the ^{11}Be + d elastic cross section as a function of the truncation angular momentum $\ell_{\max}$ in the deuteron (a) and in ^{11}Be (c), and of the maximum pseudostate energy $E_{\max}$ (b), (d). In some cases, the curves are superimposed, and a double label is used.

couplings to ensure the convergence. System (18) must be solved for each value of $J\pi$, which makes the full calculation of the cross section very long. Dealing with a very large system is a challenge for future CDCC calculations.

In Fig. 7, I analyze the elastic scattering matrix $|U_{11}^{J\pi}|$ at $E_{\rm c.m.} = 45.5$ MeV. I present results for orbital momenta $L = J - 1/2$; the alternative $L = J + 1/2$ is very similar. Four

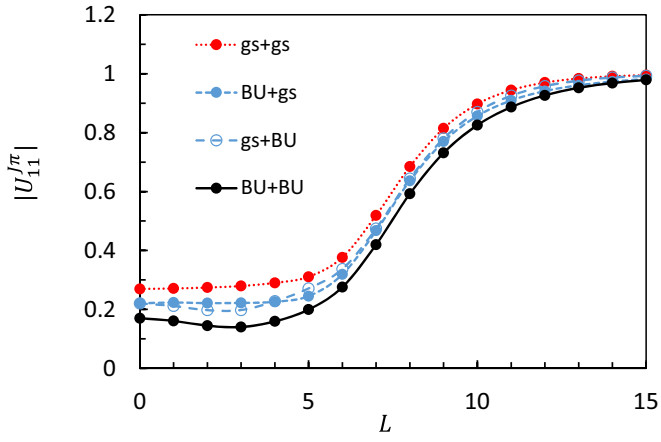

FIG. 7. Amplitude of the scattering matrix $|U_{11}^{J\pi}|$ for $L = J - 1/2$, and for different conditions of calculation (see text). Labels "gs" and "BU" refer to the ground state and to breakup channels, respectively.

calculations are presented: single-channel, mutual breakup, and breakup in ^{11}Be or in the deuteron. The general trend is a reduction of the scattering matrix when breakup channels are introduced. Including either ^{11}Be or deuteron breakup only has a similar effect, as confirmed by the cross sections shown in Ref. [12].

In Fig. 8, I display breakup cross sections corresponding to events in two energy ranges: $E_x = 0.5-3$ MeV, and $E_x = 3-5.5$ MeV. In the CDCC formalism, these cross sections are obtained by summing partial cross sections associated with pseudostates in these energy ranges. In the lower energy range, the agreement with the data is fair, but the calculation underestimates the experimental cross sections in the range $E_x = 3-5.5$ MeV. The data present a maximum near $\theta = 30^\circ$ which cannot be reproduced by theory. As for elastic scattering, the role of core excitation is weak.

V. ^{7}Li + d ELASTIC SCATTERING

Although ^{7}Li is not a weakly bound nucleus, it presents a dominant $\alpha + t$ structure, and the ^{7}Li + d system is therefore a good candidate for a four-body model. Data have been obtained, for example, in Ref. [37] at a deuteron energy $E_{\rm lab} = 25$ MeV, which corresponds to $E_{\rm c.m.} = 19.44$ MeV. This system is quite interesting in a theoretical point of view, because the four optical potentials between the fragments (α,t and p,n) are all real at low energies. Absorption is simulated by the breakup of ^{7}Li and of the deuteron. However, DWBA

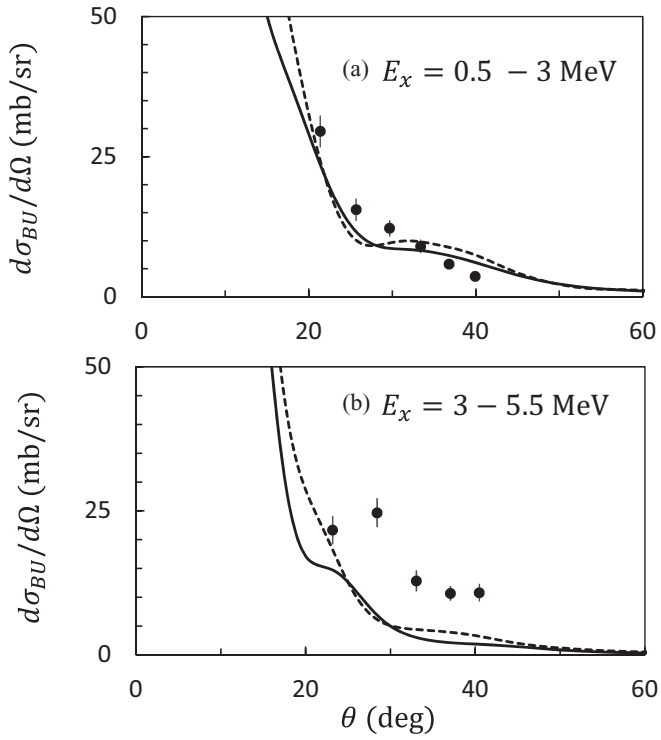

FIG. 8. $^{11}\mathrm{Be} + d$ breakup cross sections with core excitation (solid lines) and without core excitation (dashed lines). The data are taken from Ref. [11].

calculations [37] suggest that the $^7\mathrm{Li}(d,t)^6\mathrm{Li}$, and probably $^7\mathrm{Li}(d,p)^8\mathrm{Li}$, transfer channels play a role at large angles. The four-body model is therefore not expected to provide an excellent description of the cross section in a wide angular range. Compared to DWBA analyses, however, the main advantage of the present model is that there is no parameter fitting. Therefore, the predictive power is much larger than in DWBA calculations, where many parameters must be adjusted.

The ^{7}Li nucleus is described with the $\alpha + t$ potential of Ref. [38] which contains central and spin-orbit components. This potential reproduces fairly well energies and electromagnetic properties of low-lying states. For the deuteron potential, I adopt the Minnesota force [34], as for $^{11}\mathrm{Be} + d$ scattering.

The model also involves four optical potentials. The $\alpha + p$ and $\alpha + n$ potentials are taken from Ref. [39] and present a Woods-Saxon shape,

$$V_N(r) = \frac{V_0}{1 + \exp((r - R_0)/a_0)}, \tag{23}$$

with $R_0 = 2.38$ fm, $a_0 = 0.25$ fm, and $V_0 = -41.8$ MeV for $\alpha + n$, and -43 MeV for $\alpha + p$. I neglect the weak energy dependence of the parameters. I also neglect the spin-orbit term, which is a necessary approximation in CDCC calculations, where the optical parameters between the fragments should be ℓ independent.

For the $t + n$ potential, I use the nuclear part of the mirror $^3\mathrm{He} + p$ potential fitted at low energies [40]. It corresponds to $V_0 = -36.2$ MeV, $R_0 = 2.15$ fm and $a_0 = 0.144$ fm. Again I neglect the noncentral terms. The $t + p$ potential was adjusted

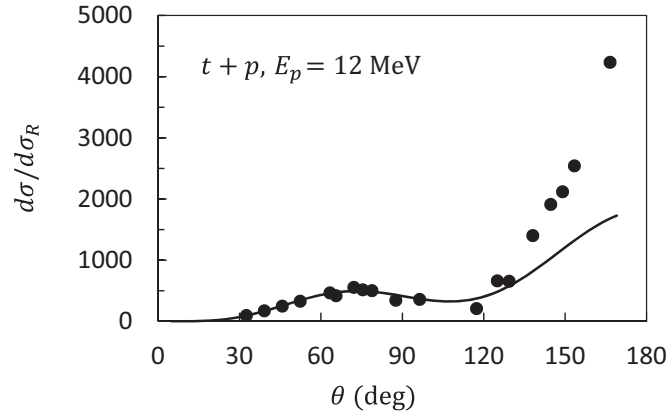

FIG. 9. Ratio to the Rutherford cross section for $t + p$ elastic scattering at $E_p = 12$ MeV (see text). The data are taken from Ref. [42].

by fine-tuning the potentials given in Ref. [41]. Parameters $V_0 = -28$ MeV, $R_0 = 2.10$ fm, and $a_0 = 0.70$ fm provide the $t + p$ elastic cross section shown in Fig. 9 for $E_p = 12$ MeV, which approximately corresponds to $E_d/2$. These optical potentials are of course necessary inputs of the model. However, the sensitivity of the $^7\mathrm{Li} + d$ cross sections is somewhat weak. Small changes in the potentials do not significantly modify the cross sections (by less than a few percents, which is hardly visible at the scale of the figure, and much less than other uncertainties associated with the model).

The $^7\mathrm{Li} + d$ elastic cross section at $E_d = 25$ MeV is shown in Fig. 10 with the data of Ref. [37]. It is computed with a maximum angular momentum $J_{\max} = 41/2$ and R-matrix parameters $a = 25$ fm and $N_f = 50$. At small angles, all calculations reproduce the data, which are dominated by the Coulomb interaction. Strong differences, however, are observed for $\theta > 30°$. Without any breakup channel, the model fails to reproduce the minimum near $\theta \simeq 35°$, and overestimates the data by 2 orders of magnitude at large angles. Introducing

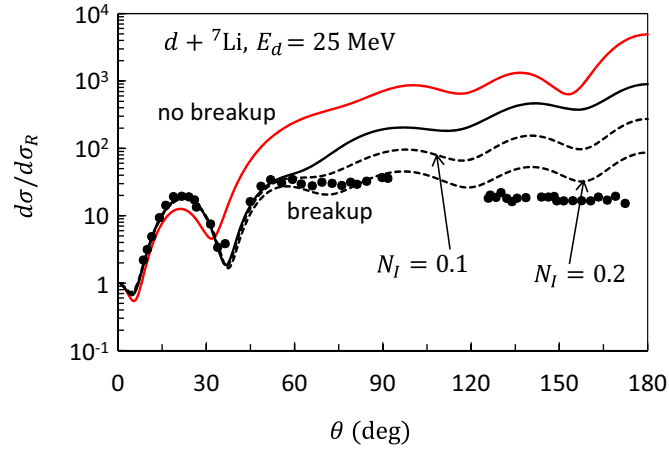

FIG. 10. Ratio to the Rutherford cross section for $^7\mathrm{Li} + d$ elastic scattering at $E_d = 25$ MeV with different conditions of calculation (see text). The dashed lines are obtained by adding the imaginary potential (25). The data are taken from Ref. [37].

breakup channels improves the agreement between theory and experiment. The behavior of the cross section up to 60° is nicely reproduced when ^{7}Li and deuteron breakup channels are introduced simultaneously. At large angles, however, the CDCC calculation still overestimates the data. Calculations have been performed by increasing the model space, but this has a minor effect on the theoretical curve.

The disagreement at large angles is consistent with the conclusion of Ref. [37] which suggests that the ^{7}Li$(d,t)^6$Li, i.e., the α transfer from ^{7}Li to ^{6}Li, is important in this angular range. To simulate this effect, missing in the present calculation, I have introduced a phenomenological imaginary part in the coupling potentials (19). This is not intended to provide a fit of the data, but rather to qualitatively assess the role of an additional imaginary potential. I therefore modify the coupling potentials (19) as

$$V^{J\pi}_{\alpha\alpha'}(R) \longrightarrow V^{J\pi}_{\alpha\alpha'}(R) + i\, W^{J\pi}_{\alpha\alpha'}(R), \tag{24}$$

and I choose the simple definition,

$$W^{J\pi}_{\alpha\alpha'}(R) = N_I\, V^{J\pi}_{\alpha\alpha'}(R), \tag{25}$$

which means that I assume the proportionality between the real and imaginary components. This approximation is often used as a first guess of the imaginary potential.

In Fig. 10, I present the calculations obtained with $N_I = 0.1$ and $N_I = 0.2$ (dashed lines). Clearly, this goes in the right direction. Except around $\theta = 150°$ where some overestimation remains, the general agreement with the data is significantly improved with $N_I = 0.2$. Of course there is no *a priori* justification of the choice $N_I = 0.2$. However, this additional imaginary part supports the suggestion that transfer channels such as ^{7}Li$(d,t)^6$Li play an important role.

The present four-body model, which does not involve any parameter fit (except, of course, in the optical potentials which are determined from independent data), represents a first step in the analysis of systems like $^7\mathrm{Li} + d$. Even if it overestimates the data at large angles, the inclusion of breakup channels in ^{7}Li and in the deuteron is fundamental.

VI. EQUIVALENT POTENTIALS

As CDCC calculations often involve many channels, it is desirable to determine equivalent potentials, which reproduce as closely as possible the CDCC cross sections. This problem was addressed in several papers (see, for example, Refs. [43–45]).

The formalism for scattering between spin zero nuclei can be found in Ref. [43], for example. I generalize here the theoretical framework when the spins are different from zero. In that case, even elastic scattering involves scattering matrices with dimension larger than one.

Let us denote as Ω the entrance channel in (14), i.e., the values c_1, c_2 of the colliding nuclei. Equation (18) can be written in a compact form as

$$(T-E)g_{\alpha(\omega)} + \sum_{\alpha'\in\Omega} V_{\alpha\alpha'} g_{\alpha'(\omega)} + \sum_{\alpha'\notin\Omega} V_{\alpha\alpha'} g_{\alpha'(\omega)} = 0, \tag{26}$$

where I drop spin and parity indices. Index ω contains the (L,I) values for the entrance channel Ω. The number of ω values is denoted as N_ω. Equation (26) therefore represents N_ω systems, each of them involving N equations. Formally this system is equivalent to the smaller system,

$$(T-E)g_{\beta(\omega)} + \sum_{\beta'\in\Omega} V^{\rm eq}_{\beta\beta'}\, g_{\beta'(\omega)} = 0, \tag{27}$$

where the equivalent potential $\boldsymbol{V}^{\rm eq}$ is now a matrix of size N_ω. Identifying Eqs. (26) and (27) provides

$$V^{\rm eq}_{\beta\beta'} = V_{\beta\beta'} + V^{\rm pol}_{\beta\beta'}, \tag{28}$$

where the polarization potential $V^{\rm pol}_{\beta\beta'}$ is given by the system,

$$\sum_{\beta'\in\Omega} V^{\rm pol}_{\beta\beta'}\, g_{\beta'(\omega)} = \sum_{\beta''\notin\Omega} V_{\beta\beta''}\, g_{\beta''(\omega)}. \tag{29}$$

The wave functions $g_{\beta(\omega)}$ are easily determined by the R-matrix method. Then the polarization potential is obtained from (29) by matrix inversion. Equation (29) is an extension of the simpler spin-zero system [43].

Of course, all potentials $(V, V^{\rm eq}, V^{\rm pol})$ depend on spin and parity. To provide a spin-independent equivalent potential, an average is performed [43] as

$$V^{\rm eq}(R) = \frac{\sum_{J\pi L} V^{{\rm eq},J\pi}_{L,L'}(R)\,\omega^{J\pi}_L(R)}{\sum_{J\pi L}\omega^{J\pi}_L(R)}, \tag{30}$$

where the weight factor $\omega^{J\pi}_L(R)$ involves the scattering matrix and the wave function as

$$\omega^{J\pi}_L(R) = (2L+1)\left(1 - \left|U^{J\pi}_{11}\right|^2\right)\left|g^L_L(R)\right|^2. \tag{31}$$

Again, Eqs. (30) and (31) are direct generalizations of simpler systems involving spin-zero nuclei. Equation (30) provides an equivalent single channel, and spin-independent, potential. It simulates the role of the breakup channels. However, it is approximative only, and the validity of this potential should be checked by comparing the cross section with the original CDCC cross section.

I present in Fig. 11 the equivalent potentials (30) for the $^{11}\mathrm{Be} + d$ system. The real part is weakly modified by the breakup channels. Only at short distances $R \lesssim 2$ fm, the real potential is affected. The situation is different for the imaginary component. Breakup channels modify the depth by a factor of two. At large distances, the imaginary potentials behave as $\sim \exp(-R/a)$ with $a \approx 0.84$ fm for the single-channel potential, and $a \approx 0.97$ fm for the full calculation. The effect of breakup channels is therefore to modify the imaginary part of the potential: The depth is larger, as well as the diffuseness of the potential. Figure 11(b) is a test of the potential. I compare the full CDCC calculations (dashed lines) with cross sections using the optical potential (30) (solid lines). The agreement is quite reasonable, which means that the optical potential of Fig. 11(a) can be considered as a good approximation of the CDCC results.

The equivalent potentials of the $^7\mathrm{Li} + d$ system are presented in Fig. 12. I consider three conditions: (1) the single-channel calculation; (2) the full calculation without additional imaginary part ($N_I = 0$); in that case the potential is real because the four optical potentials are real; (3) the full calculation using the imaginary term (27) with $N_I = 0.2$. As for

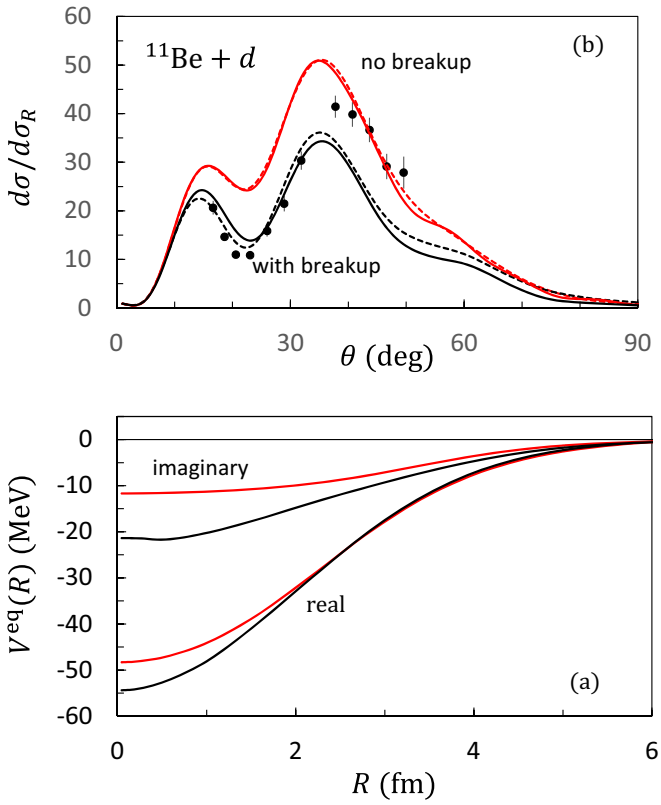

FIG. 11. (a) ^{11}Be + d equivalent potentials (30). (b) Elastic cross sections (divided by the Rutherford cross sections) with potential (30) (solid lines) and with the CDCC calculation (dashed lines). The single-channel curves are in red, and the full calculations in black.

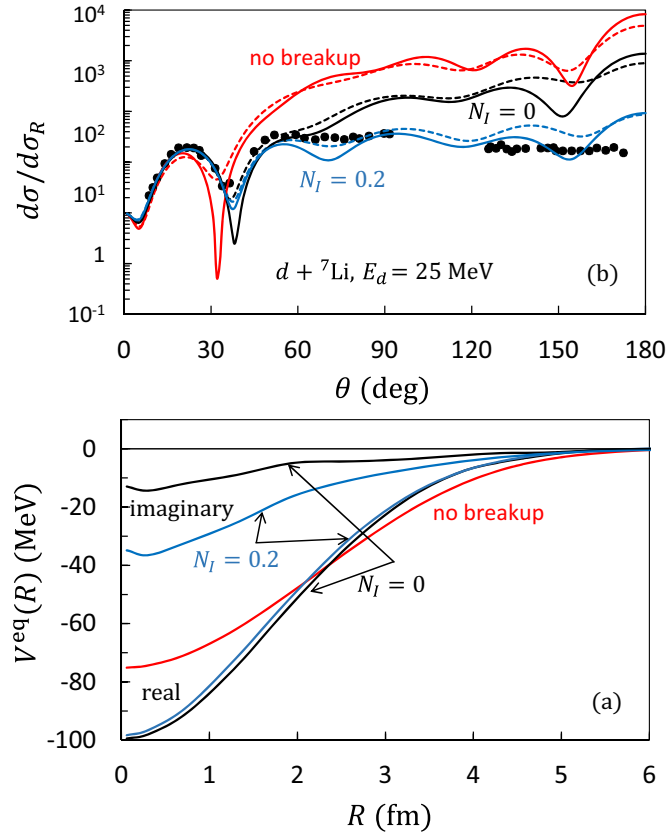

FIG. 12. See caption of Fig. 11 for the ^{7}Li + d system. Results with the imaginary potential (25) (using $N_I = 0.2$) are also shown. Notice that the imaginary potential for the single-channel calculation is exactly zero.

^{11}Be + d, the main effect of the breakup channels is to modify the imaginary component. At large distances, the asymptotic form of the imaginary potential varies as $\sim\exp(-R/a)$ with $a \approx 0.61$ fm for conditions (2), and $a \approx 0.81$ fm for conditions (3) [as mentioned before, the imaginary potential vanishes in conditions (1)]. The diffusenesses are smaller than in ^{11}Be + d because the ^{7}Li nucleus is more compact than ^{11}Be.

VII. CONCLUSION

The present work is a natural extension of the CDCC method to reactions involving two nuclei with low breakup thresholds. This situation is often met in deuteron-induced reactions on exotic nuclei. A typical example is ^{11}Be + d, where ^{11}Be is bound by 0.5 MeV only. A challenge for this approach is to deal with large channel numbers. Including pseudostates in both nuclei leads to calculations with many channels. To solve the coupled-channel system, and to derive the scattering matrices, I use the R-matrix formalism [23] associated with Lagrange functions as a basis [22]. This method provides accurate solutions, even for large systems and for closed channels. An important reduction of the computer times is obtained by using a propagation technique, where the radial interval $[0,a]$ is divided in intervals involving smaller numbers of basis functions (see Ref. [24] for details).

I have first presented a test calculation on the 4α system. The comparison with other calculations available in the literature provides a strong test of the coupling potentials. I have shown that bound-state calculations require large angular momenta and pseudostate energies in the $\alpha + \alpha$ system.

The first results on ^{11}Be + d obtained in [12] were complemented by the introduction of core excitation in ^{10}Be. As already observed in ^{11}Be + p [35], core excitation has a weak effect on the elastic scattering and breakup cross sections. In both conditions, the binding energy and the rms radius of the ground state are similar. Most likely, elastic scattering is more sensitive to these properties than to the details of the wave functions. In contrast, breakup channels are fundamental to accurately reproduce the elastic scattering data. A single-channel approach overestimates the data by about 30%. It would be interesting to have data at larger angles and at different energies to further test the precision of the model.

The ^{7}Li + d reaction is another good candidate for a four-body model. I have shown that single-channel calculations fail to reproduce experiment. When breakup channels are introduced, the data up to $\theta \approx 60^\circ$ can be nicely reproduced. However, transfer channels such as ^{7}Li(d,t)^{6}Li, are missing in the model. As an exploratory study, I introduced an additional imaginary part in the potential, and I showed that a fair agreement with experiment can be obtained.

The effect of breakup channels can be seen on the equivalent potentials. For $^{11}\mathrm{Be}+d$ as well as for $^{7}\mathrm{Li}+d$, the main effect is to increase the imaginary part of the potential. This is consistent with the picture of a stronger absorption from breakup channels.

The main advantage of the present model is its predictive power. Optical potentials between the fragments are known in most cases. Then, the cross sections are computed without any parameter fitting. A possible extension of the model would be to use the wave functions in DWBA analyses. Nucleon transfer (d,p) or (d,n) reactions are often used to investigate the structure of exotic nuclei. Such calculations represent a challenge for future scattering studies.

ACKNOWLEDGMENTS

I am grateful to A. Moro for discussions about core excitations. This work was supported by the Fonds de la Recherche Scientifique - FNRS under Grant No. 4.45.10.08. It benefited from computational resources made available on the Tier-1 supercomputer of the Fédération Wallonie-Bruxelles, infrastructure funded by the Walloon Region under the Grant Agreement No. 1117545.

APPENDIX A: TWO-BODY MATRIX ELEMENTS

In this Appendix, I discuss the matrix elements (13) involved in two-body systems. For the radial basis I use Lagrange functions [22] defined from orthogonal polynomials. A set of N functions $f_n(r)$ is given by

$$f_n(r) = \frac{1}{\sqrt{h}} F_n(r/h),$$
$$F_n(u) = (-1)^n \frac{u}{u_n}(u_n)^{1/2} \frac{L_N(u)}{u-u_n} \exp(-u/2), \quad \text{(A1)}$$

where $L_N(u)$ is the Laguerre polynomial of order N and u_n its roots. In this definition, h is a scaling parameter which can be adapted to the typical dimensions of the system. At the Gauss approximation, functions (A1) are orthogonal,

$$\langle f_n | f_{n'} \rangle \approx \delta_{nn'}, \quad \text{(A2)}$$

and the matrix elements of the kinetic energy are known analytically for various types of Lagrange meshes.

Let me discuss the matrix elements of potentials (7) by using the addition theorem,

$$P_\lambda(\cos\theta) = 4\pi(-1)^\lambda \hat{\lambda}^{-1} [Y_\lambda(\Omega) \otimes Y_\lambda(\Omega_0)]^0, \quad \text{(A3)}$$

where $\hat{\lambda} = (2\lambda+1)^{1/2}$, and where Ω and Ω_0 are the angles associated with the relative coordinate, and with the internal coordinate of the deformed nucleus, respectively. Then, a matrix element of potential (7) between basis functions (11) can be factorized as

$$\left\langle f_n \varphi^c_\gamma \middle| V \middle| f_{n'} \varphi^{c'}_{\gamma'} \right\rangle = 4\pi \sum_\lambda A^\lambda_{\gamma c,\gamma' c'} \int f_n(r) v_\lambda(r) f_{n'}(r) dr. \quad \text{(A4)}$$

Again, the use of Lagrange functions is very efficient to compute the radial part. At the Gauss approximation, the integral reads

$$\int f_n(r) v_\lambda(r) f_{n'}(r) dr \approx v_\lambda(hu_n)\delta_{nn'}. \quad \text{(A5)}$$

In Eq. (A4), some angular-momentum algebra provides

$$A^\lambda_{\gamma c,\gamma' c'} = (-1)^{I'_0+j_0+j} \hat{I}_0 \hat{j}_0 \begin{Bmatrix} I_0 & j_0 & j \\ j'_0 & I'_0 & \lambda \end{Bmatrix} C(I_0,\lambda,I'_0) \times C(\ell_0,\lambda,\ell'_0) F(\ell_0,s_0,j_0,\ell'_0,s'_0,j'_0,\lambda), \quad \text{(A6)}$$

where I use the notations,

$$C(\ell_1,\ell_2,\ell_3) = \left[\frac{(2\ell_2+1)(2\ell_3+1)}{4\pi(2\ell_1+1)}\right]^{1/2} \langle \ell_2\, 0\, \ell_3\, 0 | \ell_1 0 \rangle, \quad \text{(A7)}$$

and

$$F(\ell_0,s_0,j_0,\ell'_0,s'_0,j'_0,\lambda) = \delta_{s_0 s'_0} (-1)^{\ell_0+s_0+j'_0+\lambda} \hat{\ell}_0 \hat{j}_0 \begin{Bmatrix} j_0 & \ell_0 & s_0 \\ \ell'_0 & j'_0 & \lambda \end{Bmatrix}. \quad \text{(A8)}$$

Let me consider the matrix elements of the electric operator of order λ, defined as

$$\mathcal{M}^{\lambda\mu}(\boldsymbol{r}) = eZ_{\rm eff} r^\lambda Y^\mu_\lambda(\Omega_r), \quad \text{(A9)}$$

where the effective charge is

$$Z_{\rm eff} = Z_1 \left(-\frac{A_2}{A}\right)^\lambda + Z_2 \left(\frac{A_1}{A}\right)^\lambda. \quad \text{(A10)}$$

A reduced matrix elements between basis function (11) is given by

$$\left\langle f_n \varphi^c_\gamma \middle\| \mathcal{M}^\lambda \middle\| f_{n'} \varphi^{c'}_{\gamma'} \right\rangle = eZ_{\rm eff} B^\lambda_{\gamma c,\gamma' c'} \int f_n(r) r^\lambda f_{n'}(r) dr, \quad \text{(A11)}$$

where the radial matrix element is, at the Gauss approximation,

$$\int f_n(r) r^\lambda f_{n'}(r) dr \approx (hu_n)^\lambda \delta_{nn'}. \quad \text{(A12)}$$

The angular part is given by

$$B^\lambda_{\gamma c,\gamma' c'} = (-1)^{I_0+j_0-j+I'_0+j'_0-j'} C(\ell_0,\lambda,\ell'_0) \times F(\ell_0,s_0,j_0,\ell'_0,s'_0,j'_0,\lambda) F(j_0,I_0,j,j'_0,I'_0,j',\lambda), \quad \text{(A13)}$$

which involves coefficients defined in (A7) and (A8).

APPENDIX B: CALCULATION OF THE COUPLING POTENTIALS

In this Appendix, I provide some technical details about the calculation of the coupling potentials (19). In the first step, each fragment-fragment optical potential $V^0_{ij}(\boldsymbol{R}+\alpha\boldsymbol{r}_1+\beta\boldsymbol{r_2})$ of Eq. (2) is expanded in multipoles as

$$V^0_{ij}(\boldsymbol{R}+\alpha\boldsymbol{r}_1+\beta\boldsymbol{r_2}) = \sum_{\lambda\lambda_1\lambda_2} (-1)^\lambda \left[Y^\lambda_{\lambda_1\lambda_2}(\Omega_1,\Omega_2) \otimes Y_\lambda(\Omega_R)\right]^0 \times V_{\lambda\lambda_1\lambda_2}(R,r_1,r_2), \quad \text{(B1)}$$

where α and β are constants, and where

$$Y^{\lambda\mu}_{\lambda_1\lambda_2}(\Omega_1,\Omega_2) = \left[Y_{\lambda_1}(\Omega_1)\otimes Y_{\lambda_2}(\Omega_2)\right]^{\lambda\mu}. \tag{B2}$$

If I choose the z axis along $\boldsymbol{R}$, Eq. (B1) becomes

$$V^0_{ij}(\boldsymbol{R}+\alpha\boldsymbol{r}_1+\beta\boldsymbol{r_2}) = \frac{1}{\sqrt{4\pi}}\sum_{\lambda\lambda_1\lambda_2} Y^{\lambda 0}_{\lambda_1\lambda_2}(\Omega_1,\Omega_2)V_{\lambda\lambda_1\lambda_2}(R,r_1,r_2). \tag{B3}$$

Inverting this definition provides the multipole components of the potential,

$$V_{\lambda\lambda_1\lambda_2}(R,r_1,r_2) = \sqrt{4\pi}\int \left(Y^{\lambda 0}_{\lambda_1\lambda_2}(\Omega_1,\Omega_2)\right)^* V^0_{ij}(\boldsymbol{R}+\alpha\boldsymbol{r}_1 + \beta\boldsymbol{r_2})d\Omega_1 d\Omega_2. \tag{B4}$$

A simple calculation gives

$$V_{\lambda\lambda_1\lambda_2}(R,r_1,r_2) = (4\pi)^{3/2}\sum_{\mu\geqslant 0}(2-\delta_{\mu 0})\langle\lambda_1\,\mu\,\lambda_2\,-\mu|\lambda\,0\rangle \times\int Y^{\mu}_{\lambda_1}(\theta_1,0)\,Y^{-\mu}_{\lambda_2}(\theta_2,0)\,\cos(\mu\varphi) \times V^0_{ij}(\boldsymbol{R}+\alpha\boldsymbol{r}_1+\beta\boldsymbol{r_2})\,d(\cos\theta_1)\,d(\cos\theta_2)d\varphi, \tag{B5}$$

where φ is associated with the angle between $\boldsymbol{r}_1$ and $\boldsymbol{r}_2$, and varies in the interval $[0,\pi]$. In this definition, $\lambda+\lambda_1+\lambda_2$ must be even. These integrals involve three quadratures which are performed numerically. With expansion (B1), the matrix element (19) can be written as

$$V^{J\pi}_{\alpha\alpha'}(R) = (-1)^{I'+L+J}\hat{I}\hat{L}\sum_{\lambda\lambda_1\lambda_2}\hat{\lambda}^{-1}\begin{Bmatrix} I & L & J\\ L' & I' & \lambda\end{Bmatrix}C(L,\lambda,L') \times\sum_{\gamma_1\gamma_2\gamma_1'\gamma_2'} I_R(R;\lambda,\lambda_1,\lambda_2,j_1,j_2,j_1',j_2',\gamma_1,\gamma_2,\gamma_1',\gamma_2') \times I_\theta(\lambda,\lambda_1,\lambda_2,j_1,j_2,j_1',j_2',\gamma_1,\gamma_2,\gamma_1',\gamma_2'), \tag{B6}$$

where I use the general definition (10) for the two-body wave function. The radial term I_R is given by

$$I_R(R) = \int u^{j_1}_{\gamma_1}(r_1)u^{j_2}_{\gamma_2}(r_2)V_{\lambda\lambda_1\lambda_2}(R,r_1,r_2)u^{j_1'}_{\gamma_1'}(r_1)u^{j_2'}_{\gamma_2'}(r_2)dr_1dr_2, \tag{B7}$$

where I ignore indices of parity and of excitation level. These quadratures are simple with Lagrange functions [22].

The angular component in (B6) is the matrix element,

$$I_\theta = \left\langle\left[\varphi^{j_1}_{\gamma_1}\otimes\varphi^{j_2}_{\gamma_2}\right]^I\middle\|\left[Y_{\lambda_1}(\Omega_1)\otimes Y_{\lambda_2}(\Omega_2)\right]^\lambda\middle\|\left[\varphi^{j_1'}_{\gamma_1'}\otimes\varphi^{j_2'}_{\gamma_2'}\right]^{I'}\right\rangle, \tag{B8}$$

and reads

$$I_\theta = \hat{j}_1\hat{j}_2\hat{\lambda}\hat{I}'\begin{Bmatrix} j_1 & j_2 & I\\ \lambda_1 & \lambda_2 & \lambda\\ j_1' & j_2' & I'\end{Bmatrix}\left\langle\varphi^{j_1}_{\gamma_1}\middle\|Y_{\lambda_1}\middle\|\varphi^{j_1'}_{\gamma_1'}\right\rangle\left\langle\varphi^{j_2}_{\gamma_2}\middle\|Y_{\lambda_2}\middle\|\varphi^{j_2'}_{\gamma_2'}\right\rangle. \tag{B9}$$

Each matrix element is then given by

$$\left\langle\varphi^{j}_{\gamma}\middle\|Y_\lambda\middle\|\varphi^{j'}_{\gamma'}\right\rangle = \left\langle\left[\Phi_{I_0}\otimes\left[Y_{\ell_0}\otimes\Phi_{s_0}\right]^{j_0}\right]^j\middle\|Y_\lambda\middle\|\left[\Phi_{I_0'}\otimes\left[Y_{\ell_0'}\otimes\Phi_{s_0'}\right]^{j_0'}\right]^{j'}\right\rangle, \tag{B10}$$

and can be written as

$$\langle\varphi^{j}_{\gamma}\|Y_\lambda\|\varphi^{j'}_{\gamma'}\rangle = \delta_{I_0I_0'}\delta_{s_0s_0'}F(j_0,I_0,j,j_0',I_0',j',\lambda) \times F(\ell_0,s_0,j_0,\ell_0',s_0',j_0',\lambda)C(\ell_0,\lambda,\ell_0'), \tag{B11}$$

where I have used definitions (A6) and (A7). The calculation of the coupling potentials (19) can therefore be divided in several steps, each of which being fairly simple. Of course, these expressions strongly simplify in the standard case with no core excitation ($I_0 = I_0' = 0$). Global tests can be performed on the Coulomb potential because, at large distances, the multipole expansion (B1) is known analytically. Then, the coupling Coulomb potentials are defined from matrix elements of the multipole operators in nuclei 1 and 2.

[1] G. H. Rawitscher, Phys. Rev. C **9**, 2210 (1974).
[2] M. Kamimura, M. Yahiro, Y. Iseri, S. Sakuragi, H. Kameyama, and M. Kawai, Prog. Theor. Phys. Suppl. **89**, 1 (1986).
[3] N. Austern, Y. Iseri, M. Kamimura, M. Kawai, G. Rawitscher, and M. Yahiro, Phys. Rep. **154**, 125 (1987).
[4] M. Yahiro, K. Ogata, T. Matsumoto, and K. Minomo, Prog. Theor. Exp. Phys. **2012**, 01A206 (2012).
[5] T. Matsumoto, E. Hiyama, K. Ogata, Y. Iseri, M. Kamimura, S. Chiba, and M. Yahiro, Phys. Rev. C **70**, 061601 (2004).
[6] P. Descouvemont, T. Druet, L. F. Canto, and M. S. Hussein, Phys. Rev. C **91**, 024606 (2015).
[7] J. P. Fernández-García, M. Cubero, L. Acosta, M. Alcorta, M. A. G. Alvarez, M. J. G. Borge, L. Buchmann, C. A. Diget, H. A. Falou, B. Fulton, H. O. U. Fynbo, D. Galaviz, J. Gómez-Camacho, R. Kanungo, J. A. Lay, M. Madurga, I. Martel, A. M. Moro, I. Mukha, T. Nilsson, M. Rodríguez-Gallardo, A. M. Sánchez-Benítez, A. Shotter, O. Tengblad, and P. Walden, Phys. Rev. C **92**, 044608 (2015).
[8] R. Kanungo, A. Gallant, M. Uchida, C. Andreoiu, R. Austin, D. Bandyopadhyay, G. Ball, J. Becker, A. Boston, H. Boston, B. Brown, L. Buchmann, S. Colosimo, R. Clark, D. Cline, D. Cross, H. Dare, B. Davids, T. Drake, M. Djongolov, P. Finlay, N. Galinski, P. Garrett, A. Garnsworthy, K. Green, S. Grist, G. Hackman, L. Harkness, A. Hayes, D. Howell, A. Hurst, H. Jeppesen, K. Leach, A. Macchiavelli, D. Oxley, C. Pearson, B. Pietras, A. Phillips, S. Rigby, C. Ruiz, G. Ruprecht, F. Sarazin, M. Schumaker, A. Shotter, C. Sumitharachchi, C. Svensson, I. Tanihata, S. Triambak, C. Unsworth, S. Williams, P. Walden, J. Wong, and C. Wu, Phys. Lett. B **682**, 391 (2010).
[9] Y. Suzuki and M. Takahashi, Phys. Rev. C **65**, 064318 (2002).
[10] N. K. Timofeyuk, Phys. Rev. C **78**, 054314 (2008).

[11] J. Chen, J. L. Lou, Y. L. Ye, J. Rangel, A. M. Moro, D. Y. Pang, Z. H. Li, Y. C. Ge, Q. T. Li, J. Li, W. Jiang, Y. L. Sun, H. L. Zang, Y. Zhang, N. Aoi, E. Ideguchi, H. J. Ong, J. Lee, J. Wu, H. N. Liu, C. Wen, Y. Ayyad, K. Hatanaka, T. D. Tran, T. Yamamoto, M. Tanaka, T. Suzuki, and T. T. Nguyen, Phys. Rev. C **94**, 064620 (2016).

[12] P. Descouvemont, Phys. Lett. B **772**, 1 (2017).

[13] Y. Ogawa, K. Arai, Y. Suzuki, and K. Varga, Nucl. Phys. A **673**, 122 (2000).

[14] R. L. Varner, W. J. Thompson, T. L. McAbee, E. J. Ludwig, and T. B. Clegg, Phys. Rep. **201**, 57 (1991).

[15] A. J. Koning and J. P. Delaroche, Nucl. Phys. A **713**, 231 (2003).

[16] A. Di Pietro, V. Scuderi, A. M. Moro, L. Acosta, F. Amorini, M. J. G. Borge, P. Figuera, M. Fisichella, L. M. Fraile, J. Gomez-Camacho, H. Jeppesen, M. Lattuada, I. Martel, M. Milin, A. Musumarra, M. Papa, M. G. Pellegriti, F. Perez-Bernal, R. Raabe, G. Randisi, F. Rizzo, G. Scalia, O. Tengblad, D. Torresi, A. M. Vidal, D. Voulot, F. Wenander, and M. Zadro, Phys. Rev. C **85**, 054607 (2012).

[17] R. de Diego, R. Crespo, and A. M. Moro, Phys. Rev. C **95**, 044611 (2017).

[18] J. A. Lay, R. de Diego, R. Crespo, A. M. Moro, J. M. Arias, and R. C. Johnson, Phys. Rev. C **94**, 021602 (2016).

[19] N. C. Summers, F. M. Nunes, and I. J. Thompson, Phys. Rev. C **74**, 014606 (2006).

[20] I. J. Thompson, Comput. Phys. Rep. **7**, 167 (1988).

[21] Y. Sakuragi, M. Yahiro, and M. Kamimura, Prog. Theor. Phys. Suppl. **89**, 136 (1986).

[22] D. Baye, Phys. Rep. **565**, 1 (2015).

[23] P. Descouvemont and D. Baye, Rep. Prog. Phys. **73**, 036301 (2010).

[24] P. Descouvemont, Comput. Phys. Commun. **200**, 199 (2016).

[25] A. M. Lane and R. G. Thomas, Rev. Mod. Phys. **30**, 257 (1958).

[26] P. Burke, *R-Matrix Theory of Atomic Collisions. Application to Atomic, Molecular and Optical Processes*, Springer Series on Atomic, Optical, and Plasma Physics, Vol. 61 (Springer, Berlin, Heidelberg, 2011).

[27] S. Ali and A. R. Bodmer, Nucl. Phys. **80**, 99 (1966).

[28] E. M. Tursunov, D. Baye, and P. Descouvemont, Nucl. Phys. A **723**, 365 (2003).

[29] W. Horiuchi, private communication.

[30] P. Capel, G. Goldstein, and D. Baye, Phys. Rev. C **70**, 064605 (2004).

[31] N. C. Summers, S. D. Pain, N. A. Orr, W. N. Catford, J.-C. Angélique, N. I. Ashwood, V. Bouchat, N. M. Clarke, N. Curtis, M. Freer, B. R. Fulton, F. Hanappe, M. Labiche, J. L. Lecouey, R. C. Lemmon, D. Mahboub, A. Ninane, G. Normand, F. M. Nunes, N. Soić, L. Stuttge, C. N. Timis, I. J. Thompson, J. S. Winfield, and V. Ziman, Phys. Lett. B **650**, 124 (2007).

[32] E. Kwan, C. Y. Wu, N. C. Summers, G. Hackman, T. E. Drake, C. Andreoiu, R. Ashley, G. C. Ball, P. C. Bender, A. J. Boston, H. C. Boston, A. Chester, A. Close, D. Cline, D. S. Cross, R. Dunlop, A. Finlay, A. B. Garnsworthy, A. B. Hayes, A. T. Laffoley, T. Nano, P. Navrátil, C. J. Pearson, J. Pore, S. Quaglioni, C. E. Svensson, K. Starosta, I. J. Thompson, P. Voss, S. J. Williams, and Z. Wang, Phys. Lett. B **732**, 210 (2014).

[33] W. Nörtershäuser, D. Tiedemann, M. Žáková, Z. Andjelkovic, K. Blaum, M. L. Bissell, R. Cazan, G. W. F. Drake, C. Geppert, M. Kowalska, J. Krämer, A. Krieger, R. Neugart, R. Sánchez, F. Schmidt-Kaler, Z.-C. Yan, D. T. Yordanov, and C. Zimmermann, Phys. Rev. Lett. **102**, 062503 (2009).

[34] D. R. Thompson, M. LeMere, and Y. C. Tang, Nucl. Phys. A **286**, 53 (1977).

[35] J. Chen, J. L. Lou, Y. L. Ye, Z. H. Li, Y. C. Ge, Q. T. Li, J. Li, W. Jiang, Y. L. Sun, H. L. Zang, N. Aoi, E. Ideguchi, H. J. Ong, Y. Ayyad, K. Hatanaka, D. T. Tran, T. Yamamoto, M. Tanaka, T. Suzuki, N. T. Tho, J. Rangel, A. M. Moro, D. Y. Pang, J. Lee, J. Wu, H. N. Liu, and C. Wen, Phys. Rev. C **93**, 034623 (2016).

[36] M. Rhoades-Brown, M. H. Macfarlane, and S. C. Pieper, Phys. Rev. C **21**, 2417 (1980).

[37] N. Burtebayev, J. T. Burtebayeva, A. Duisebayev, Z. K. Kerimkulov, M. Nassurlla, T. Zholdybayev, S. V. Artemov, A. A. Karakhodzhayev, U. S. Salikhbayev, S. B. Sakuta, S. Kliczewski, E. Piasecki, K. Rusek, R. Siudak, A. Trzcinska, M. Wolinska-Cichocka, and A. Amar, Acta Phys. Pol. B **46**, 1037 (2015).

[38] B. Buck and A. C. Merchant, J. Phys. G **14**, L211 (1988).

[39] S. Ali, A. A. Z. Ahmad, and N. Ferdous, Rev. Mod. Phys. **57**, 923 (1985).

[40] H. S. Sherif, Phys. Rev. C **19**, 1649 (1979).

[41] A. Pakou, F. Cappuzzello, N. Keeley, L. Acosta, C. Agodi, X. Aslanoglou, S. Calabrese, D. Carbone, M. Cavallaro, A. Foti, G. Marquínez-Durán, I. Martel, M. Mazzocco, C. Parascandolo, D. Pierroutsakou, K. Rusek, O. Sgouros, V. Soukeras, E. Strano, V. A. B. Zagatto, and K. Zerva, Phys. Rev. C **96**, 034615 (2017).

[42] R. Kankowsky, J. C. Fritz, K. Kilian, A. Neufert, and D. Fick, Nucl. Phys. A **263**, 29 (1976).

[43] I. Thompson, M. Nagarajan, J. Lilley, and M. Smithson, Nucl. Phys. A **505**, 84 (1989).

[44] R. S. Mackintosh and N. Keeley, Phys. Rev. C **70**, 024604 (2004).

[45] J. Lubian and F. M. Nunes, J. Phys. G **34**, 513 (2007).